

Ultrafast Carrier Dynamics in VO₂ across the Pressure-Induced Insulator-to-Metal Transition

Johannes M. Braun,^{1,2,*} Harald Schneider,¹ Manfred Helm,^{1,2} Rafał Mirek,³
Lynn A. Boatner,⁴ Robert E. Marvel,⁵ Richard F. Haglund,⁵ and Alexej Pashkin^{1,†}

¹*Helmholtz-Zentrum Dresden-Rossendorf, P.O. Box 510119, 01314 Dresden, Germany*

²*Technische Universität Dresden, 01062 Dresden, Germany*

³*Faculty of Physics, University of Warsaw, Pasteura 5, PL-02-093 Warsaw, Poland*

⁴*Oak Ridge National Laboratory, P.O. Box 2008, Oak Ridge, TN 37831, USA*

⁵*Vanderbilt University, Department of Physics and Astronomy, Nashville, TN 37235-1807, USA*

(Dated: March 13, 2022)

We utilize near-infrared pump – mid-infrared probe spectroscopy to investigate the ultrafast electronic response of pressurized VO₂. Distinct pump–probe signals and a pumping threshold behavior are observed even in the pressure-induced metallic state showing a noticeable amount of localized electronic states. Our results are consistent with a scenario of a bandwidth-controlled Mott-Hubbard transition.

Vanadium dioxide (VO₂) exhibits a sharp insulator-to-metal transition (IMT) accompanied by a transformation from the monoclinic to rutile crystal structure above a critical temperature $T_c = 340$ K [1]. The strong coupling between electronic and lattice subsystems during the phase transition has attracted continuing interest for more than a half century [2–4]. The dimerized vanadium chains of the monoclinic phase suggests that a Peierls distortion underlies the insulating state, but electronic correlation leading to the carrier localization typical of a Mott insulator is also observed [5–8]. The IMT in VO₂ under the influence of temperature [6, 9–11], strain [12–14] and chemical substitution [15, 16] has been extensively studied. Some of these studies show that the electronic and structural phase transitions are separable within certain temperature ranges, pointing to a primary role for electron correlation as the driving mechanism for the IMT [10, 12].

Application of external pressure offers an attractive way to distinguish the influence of the structural instability from the correlation effects on the IMT in VO₂. At sufficiently high pressures, VO₂ becomes metallic while keeping the dimerized monoclinic structure [17–22]. External pressure induces only an isostructural transformation of the lattice at room temperature [21–23]. Thus, in this case the pressure-driven IMT should be dominated by changes in the electronic band structure which is necessarily different from that of the temperature-induced IMT. Therefore, it is highly desirable to unravel how the band structure of the monoclinic metallic phase VO₂ changes under high pressure. Unfortunately, in a high-pressure diamond anvil cell (DAC), conventional photoemission spectroscopy cannot be used, and X-ray absorption spectroscopy suffers from limited energy resolution [19].

Information about the electron and lattice dynamics in VO₂ can be obtained using time-resolved techniques that probe the evolution of the non-thermal IMT [10, 24–35]. In particular, time-resolved photoemission spec-

troscopy [32] and ultrafast electron diffraction [33] have shown that a transient monoclinic but metallic phase can be induced via photoexcitation. A *transient* monoclinic metallic phase has also been reported for pressurized VO₂ [36] using time-resolved reflectivity.

Here we combine an ultrafast near-infrared pump and mid-infrared spectroscopy in a high-pressure DAC to investigate the non-equilibrium dynamics of the pressure-induced IMT in VO₂. Our results provide evidence that near-infrared pumping induces additional long-lived charge carriers – even in the pressure-induced metallic phase. The utilized method of the non-degenerate non-linear spectroscopy enables us to trace the evolution of localized, weakly localized and fully delocalized electronic states in VO₂ across the pressure-driven IMT, and to draw conclusions about the appropriate correlated band structure.

We use VO₂ single crystals grown by thermal decomposition of V₂O₅ [11, 37]. The samples were polished to thicknesses of 20–30 μm and cut into pieces of around 100 μm in diameter. A single piece of VO₂ was mounted in an opposing-plate DAC. CsI powder was used as a pressure transmitting medium in order to ensure a direct contact between the sample surface and the front diamond anvil. The pressure inside the DAC was monitored via a standard ruby fluorescence method [38].

Our pump–probe setup is based on a Ti:sapphire laser amplifier system, providing 55 fs long pulses centered at $\lambda \approx 800$ nm (1.55 eV) with a repetition rate of 250 kHz. A portion of the beam was used for the pumping branch, whereas the remaining part was utilized to generate probe pulses at $\lambda = 10$ μm (0.12 eV or 30 THz) using difference frequency mixing between signal and idler pulses from a parametric amplifier. The pump and probe beams were focused non-collinearly on the sample inside the DAC down to a spot size of 30–50 μm (FWHM). We then measure the change in reflectivity ΔR of photo-excited VO₂ with respect to the reflectivity R in the unexcited state. The small photon energy of the probe beam (well

below the band gap energy $E_g = 0.6$ eV of VO₂ at ambient conditions) ensures that the pump–probe signal is dominated by the response of free charge carriers [28, 29].

Figure 1(a) shows the change of the pump–probe signal of VO₂ at 2.1 GPa measured for different pump fluences. All of the curves show a quasi-instantaneous increase of the reflectivity – limited only by the durations of the pump and the probe pulses. The onset is followed by a fast relaxation with a time constant of approximately 0.2 ps [37]. At low fluence (green trace), the pump–probe signal vanishes after about 1 ps indicating a return to complete localization of the photo-excited charge carriers. At pump fluences above a threshold Φ_{th} a persistent enhanced reflectivity reveals the creation of a metastable metallic phase [see the orange and red trace in Fig. 1(a)]. This state survives for hundreds of picoseconds in agreement with previous studies [27, 39, 40]. All of these observations are fully consistent with the results for ambient conditions published previously [28]. The threshold fluence Φ_{th} corresponds to the photoinjection of a critical density of free charge carriers that screen the Coulomb interaction and thus induce the collapse of the energy gap, thus leading to the metastable metallic state [10, 28, 32].

The volume of the metastable metallic phase and correspondingly the amplitude of the persistent pump–probe signal grows, when the incident pump fluence Φ is increased above the threshold Φ_{th} . This is related to the fact that the penetration depth of the mid-infrared probe and the sample thickness are much larger than the absorption length of the near-infrared pump; the photoexcitation switches only a relatively thin surface layer of the VO₂ crystal.

Remarkably, in contrast to the low-pressure regime, at elevated pressures the long-lived excited state is already observed at pump fluences below the threshold as shown in Fig. 1(b). This becomes more obvious when we plot pump–probe signals averaged around 1 ps (where the relaxation process is already completed) as a function of the pump fluence. Figures 1(c) and 1(d) show such plots for the same pressures as for Fig. 1(a) and 1(b), respectively. The threshold behavior is clearly seen in both cases. In contrast to previous works [28–30], the threshold is no longer well-defined by the crossing of the high-fluence asymptote with the x-axis, since finite signals are observed down to the lowest pump fluences. Therefore, we define Φ_{th} as a crossing point (marked by red arrows) of the two asymptotes (dashed gray lines) illustrated in Fig. 1(c) and (d). Details of the bi-asymptotic fit function are given in [37].

The analysis of pump–probe traces at different pump fluences and various pressures reveals two main parameters that exhibit anomalous pressure behavior: (i) threshold fluence Φ_{th} and (ii) slope of the low-fluence asymptote denoted as m_1 [37]. Figure 2 shows the pressure dependence of these key parameters together with the linear (unpumped) transmissivity and reflectivity at the

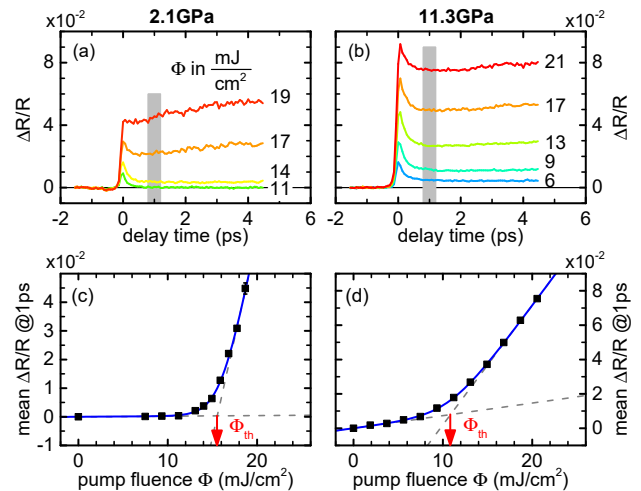


FIG. 1. (color online). Calibrated pump–probe signals for different pump fluences Φ at $T = 300$ K and hydrostatic pressure of (a) 2.1 GPa and (b) 11.3 GPa. Time-averaged pump–probe signals for delay times between 0.8 and 1.2 ps [highlighted as grey area in (a) and (b)] versus pump fluence for (c) 2.1 GPa and (d) 11.3 GPa. Black squares represent experimental data, the blue lines show corresponding fits. The crossing point of the asymptotes of the fits (dashed lines) determine the threshold fluence Φ_{th} .

probe photon energy. Starting from ambient pressure, the threshold fluence Φ_{th} monotonically increases up to a critical pressure p_c of 6–8 GPa as shown in Fig. 2(a). A higher threshold fluence means that more free carriers have to be photoinjected to overcome the correlations and to induce the metastable metallic state. This trend contrasts sharply with the behavior of the thermally driven IMT where a noticeable decrease of the threshold fluence on approaching T_c has been reported [29, 30]. Most probably this difference is related to the stiffening of the dimerized lattice structure under pressure; that makes the vanadium dimers even more stable and thus raises the energy barrier to the metallic rutile phase. A stiffening of phonons observed in the pressure-dependent Raman measurements [17, 21] as well as enhanced dimerization of the vanadium sublattice seen in X-ray scattering [20] confirm this interpretation. Furthermore, the observed increase of Φ_{th} with pressure is consistent with the recently reported growth of T_c in VO₂ under pressure and the estimations of the corresponding increase in the latent heat of the IMT [22].

Around the critical pressure p_c we observe an anomalous drop of Φ_{th} . Remarkably, it coincides with the vanishing of the linear transmissivity [Fig. 2(c)], the start of the increase in the reflectivity [Fig. 2(d)] as well as the onset of a finite slope m_1 of the low-fluence asymptote [Fig. 2(b)]. This effect is highly reproducible and has been observed in independent measurements on three different VO₂ samples as presented in Fig. 2. We interpret the observed anomaly as a pressure-driven IMT in

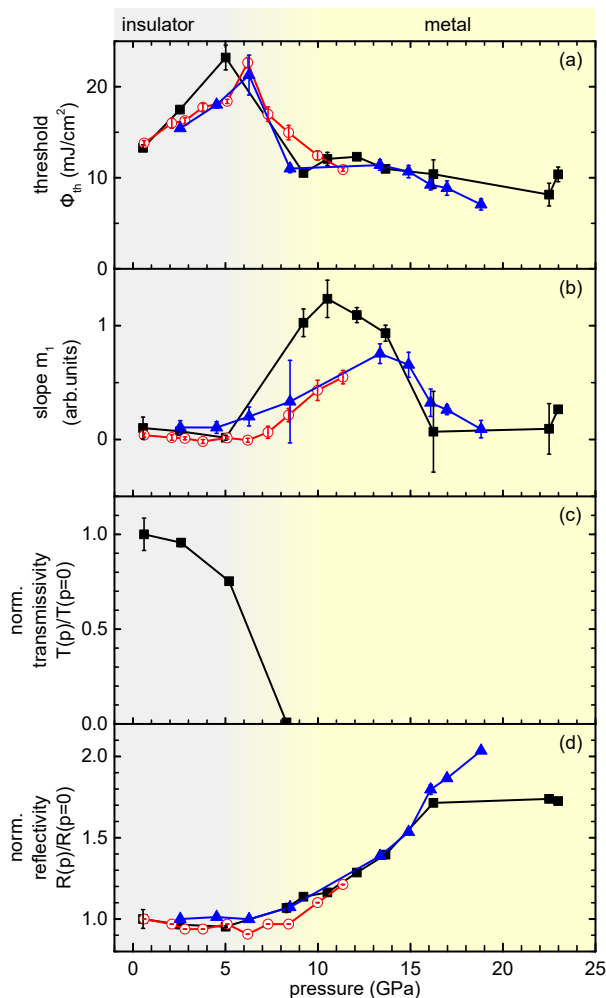


FIG. 2. (color online). (a) Threshold fluence Φ_{th} and (b) slope m_1 obtained from the fitting as functions of pressure for three different VO_2 crystals (corresponding to different colors and symbols). (c) Normalized linear transmissivity and (d) reflectivity of VO_2 versus pressure.

VO_2 . Our results for the linear mid-infrared response agree with the work of Arcangeletti *et al.* [17] where this phenomenon was reported for the first time. The sharper drop in our transmission-versus-pressure data can be explained by the much larger thickness of our sample. The reflectivity starts to increase for $p > p_c$ due to the presence of delocalized charge carriers and continues to grow as their density and correspondingly the plasma frequency become larger. In agreement with previous reports [17, 18, 21, 23], our complementary high-pressure Raman measurements confirm that VO_2 samples also preserve the monoclinic crystal structure far above p_c [37].

Let us now discuss the nonlinear response of VO_2 in the pressure-induced metallic state. The similar shape of the pump-probe response beyond the critical pressure p_c [see Fig. 1(b)] indicates that the majority of vanadium

d -electrons remain localized even in the pressure-driven metallic phase and a photoexcitation is still able to induce a phase with a higher conductivity. Moreover, the finite values of the threshold fluence [see Fig. 2(a)] suggest that the photo-induced metallization for $p > p_c$ is governed by the same mechanism as for pressures below p_c . The observed drop of Φ_{th} above the IMT can be related to the finite pressure-induced density of free charge carriers that should lead to a partial screening of the Coulomb correlation. As a result, fewer photoinjected carriers are required to achieve the critical concentration that closes the band gap.

A further increase of pressure up to 23 GPa causes gradual lowering of Φ_{th} indicating that the density of free charge carriers grows with pressure. Nevertheless, it remains below the critical concentration necessary for complete suppression of the carrier localization. This is consistent with the behavior of the pressure-dependent reflectivity that monotonically increases up to the highest pressures – suggesting that the plasma frequency of free charge carriers just slightly exceeds the frequency of our mid-infrared probe. Assuming an electron mass $m^* \approx 2m_e$ [6], we estimate the density of free electrons to be roughly $2 \times 10^{20} \text{ cm}^{-3}$ – still a factor five lower than the critical concentration of 10^{21} cm^{-3} needed for the photo-induced phase transition at ambient pressure [29]. At high pressures, the critical concentration may be even higher. Thus, the equilibrium density of free carriers for $p > p_c$ is still well below the critical limit, that could be the reason for the quite moderate decrease of the threshold beyond p_c .

The pressure-induced IMT also leads to the onset of a non-vanishing slope m_1 of the low-fluence asymptote [see Fig. 2(b)]. This means that for $p > p_c$ even pumping well below a threshold fluence can induce a metastable metallic phase with enhanced reflectivity, as illustrated in Fig. 1(b). In other words, a certain amount of long-lived free charge carriers directly proportional to the number of pump photons can be added without reaching the critical concentration for a band gap collapse. Thus, the appearance of a finite m_1 is expected to be a *non-cooperative phenomenon* related to the photoexcitation of weakly localized states (WLS) located near the Fermi level.

The observed behavior of the pump-probe response across the pressure-driven IMT can be understood on the basis of the tentative band diagrams depicted in Fig. 3(a)-(c). Figure 3(a) shows the band structure of VO_2 at ambient conditions established in previous studies [2, 5, 9]. The t_{2g} vanadium orbitals overlapping along the a_M axis [29] form two relatively narrow bands usually denoted as d_{\parallel} . The low- and the high-energy bands correspond to bonding and antibonding combinations of electronic orbitals on a vanadium dimer, respectively. Due to the on-site Coulomb repulsion U of t_{2g} electrons, the lower and upper Hubbard bands are formed on the lower and upper energy ends of the d_{\parallel} bands, respectively

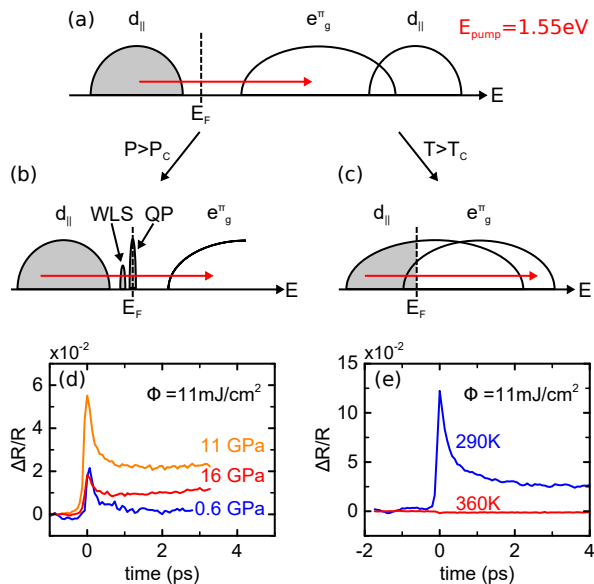


FIG. 3. (color online). (a), (b) and (c) schematic energy bands of VO_2 for (a) insulating monoclinic phase at ambient conditions ($T < T_c$ and $p < p_c$), (b) pressure-driven metallic phase and (c) temperature-driven metallic rutile phase. The qualitative drawing of the density of states (DOS) as function of the energy E is restricted to the surrounding of the Fermi energy E_F ; in (b) appear weakly localized states (WLS) and a quasiparticle peak (QP), while the upper Hubbard band is above the shown energy scale. (d) calibrated pump-probe signal in reflectivity for different pressures p at $T = 300$ K and pump fluence $\Phi = 11$ mJ/cm^2 . (e) calibrated pump-probe signal in reflectivity at ambient pressure and $\Phi = 11$ mJ/cm^2 for $T < T_c$ (blue line) and $T > T_c$ (red line).

[5]. In our qualitative band diagrams, we present both bands as somewhat broader d_{\parallel} bands. The band gap is formed between edges of the lower d_{\parallel} band and the e_g^{π} band. Photoexcitation promotes the localized electrons from the d_{\parallel} band into the high-energy delocalized states [red arrow in Fig. 3(a)] leading to the transient increase of reflectivity.

In our measurements, we observe photo-induced free charge carriers typical of the insulating VO_2 phase well above the pressure-induced IMT – in stark contrast to the temperature-induced transition. This difference becomes clear by comparing the pump-probe signals measured on our VO_2 using the same excitation fluence for different pressures [Fig. 3(d)] and for different temperatures [Fig. 3(e)]. For temperatures above T_c , the metallic VO_2 phase possesses the rutile crystal structure without the dimerization. Thus, d_{\parallel} bands become degenerate and cross the Fermi level together with other t_{2g} bands [see Fig. 3(c)] resulting in a complete delocalization of all $3d$ electrons of vanadium ions. Therefore, the photoexcitation increases the electronic temperature, but it does not lead to an increase in the total number of free charge carriers. Correspondingly we observe a very weak negative

change in $\Delta R/R$ for $T > T_c$ as shown by the red trace in Fig. 3(e). In contrast to this, the pressure-induced metallic state of VO_2 is monoclinic [37] suggesting that the d_{\parallel} bands remain split. The drop of the threshold fluence leads to an enhanced photosusceptibility [37], and the sizable pump-induced $\Delta R/R$ for $p > p_c$ signals shown in Fig. 3(d) indicate that a large part of the $3d$ electrons are localized, i.e., they occupy states in a band which does not cross the Fermi level. This assumption is supported by the X-ray absorption measurements by Marini *et al.* [19] which show that the spectral weight transfer needed to achieve the pressure-induced metallic monoclinic phase is much smaller than for the temperature-driven transition to the rutile phase.

In addition, as discussed above, the appearance of finite m_1 values suggests the existence of weakly localized states WLS for $p > p_c$. These conclusions result in the tentative band diagram shown in Fig. 3(b). It assumes that the band splitting is also preserved above the pressure-induced IMT, and the metallic conductivity originates from a spectral weight transfer to a narrow intragap quasiparticle peak (QP) at the Fermi level. Its low-energy satellite represents the WLS. At elevated pressures well above p_c , the QP gains more spectral weight leading to higher metallic conductivity in line with the observed increase in reflectivity [Fig. 2(d)]. At the same time, the pump-probe signal $\Delta R/R$ becomes smaller since the photo-induced relative change in the density of free charge carriers decreases for a given pump fluence [see the decrease from orange to red trace in Fig. 3(d)]. Finally, m_1 vanishes at high pressures [Fig. 2(b)] indicating that the WLS merges with the QP.

We now discuss the scenario of the pressure-induced IMT in VO_2 via the suggested band diagram. Our data convincingly demonstrate that the dimerized monoclinic structure is preserved across the IMT and even becomes more stable under an initial pressure increase. Thus, the intimate coupling between the electronic and lattice subsystems characteristic of the temperature-driven IMT does not take place for the pressure-induced IMT which should have a predominantly electronic origin. The simplest scenario in this case is an IMT in the nondegenerate Hubbard model. Single-site dynamical mean field theory (DMFT) calculations for such model show that an increasing portion of spectral weight is transferred from the lower and upper Hubbard bands to a quasiparticle peak at the Fermi level when the effective correlation drops below a critical value, while the Hubbard bands persist [41, 42]. The onset of the QP and the redistribution of spectral weight are governed by the ratio of the Coulomb repulsion U and the hopping bandwidth t [42].

Application of pressure improves the overlap between the orbitals leading to increased bandwidth t and reduced effective correlation U/t that eventually results in a bandwidth-controlled Mott-Hubbard insulator-to-metal transition. Thus, this simple model is capable

of explaining the existence of the localized states in the lower-energy band even above the IMT as suggested by our present study [Fig. 3(b)]. The only discrepancy is related to the existence of the WLS that are absent for the bandwidth-controlled IMT in the standard nondegenerate Hubbard model in single-site DMFT [41, 42].

We expect two possible reasons to be responsible for the appearance of WLS: (i) The WLS may be caused by lattice defects in the VO₂ crystal. Possibly their density increases notably due to the high strain imposed by external pressure [34]. Initially delocalized electrons in the narrow QP are known to possess a high effective mass due to strong correlation effects [6, 42] and, thus, may be localized and bound to lattice defects. With further increasing pressure and weaker correlation, the effective mass should strongly decrease such that the binding energy of the localized states may drop below the energy of thermal fluctuations at room temperature. As a result, the bound states will be ionized and the WLS peak will merge with the QP. (ii) The WLS may be an intrinsic feature of a realistic Hubbard model which goes beyond the single-site approximation and includes all relevant bands in VO₂ and must be solved using contemporary calculation techniques [5, 43, 44]. Unfortunately, to the best of our knowledge, no such modeling has yet been performed for a pressure-induced metallic phase of VO₂.

In conclusion, we have observed a pressure-induced metallic monoclinic phase of VO₂ above a critical pressure p_c of 6-8 GPa by using nonlinear pump-probe spectroscopy. The photo-induced response of VO₂ above the pressure-induced IMT is remarkably different as compared to the temperature-driven transition. This behavior agrees well with the scenario of a bandwidth-controlled Mott-Hubbard transition, where the strongly correlated metallic phase appears due to a spectral weight transfer from the Hubbard bands to delocalized states at the Fermi level. Thus, the application of external pressure provides a structural stability of VO₂ and reveals the purely electronic character of the insulator-to-metal phase transition.

We thank A. Leitenstorfer and P.M. Oppeneer for fruitful discussions and support. This work was financially supported by the DFG (project 2113-1/1: A.P., J.M.B.). Research at the Oak Ridge National Laboratory for one author (L.A.B.) was supported by the U.S. Department of Energy, Office of Science, Basic Energy Sciences, Materials Sciences and Engineering Division. REM and RFH gratefully acknowledge funding from the National Science Foundation (DMR-1207507).

* j.braun@hzdr.de

† a.pashkin@hzdr.de

[1] F. J. Morin, Phys. Rev. Lett. **3**, 34 (1959).

- [2] J. B. Goodenough, J. Solid State Chem. **3**, 490 (1971).
- [3] M. Imada, A. Fujimori, and Y. Tokura, Rev. Mod. Phys. **70**, 1039 (1998).
- [4] D. N. Basov, R. D. Averitt, D. van der Marel, M. Dressel, and K. Haule, Rev. Mod. Phys. **83**, 471 (2011).
- [5] S. Biermann, A. Poteryaev, A. I. Lichtenstein, and A. Georges, Phys. Rev. Lett. **94**, 026404 (2005).
- [6] M. M. Qazilbash, M. Brehm, B.-G. Chae, P.-C. Ho, G. O. Andreev, B.-J. Kim, S. J. Yun, A. V. Balatsky, M. B. Maple, F. Keilmann, H.-T. Kim, and D. N. Basov, Science **318**, 1750 (2007).
- [7] C. Weber, D. D. O'Regan, N. D. M. Hine, M. C. Payne, G. Kotliar, and P. B. Littlewood, Phys. Rev. Lett. **108**, 256402 (2012).
- [8] T. J. Huffman, C. Hendriks, E. J. Walter, J. Yoon, H. Ju, R. Smith, G. L. Carr, H. Krakauer, and M. M. Qazilbash, Phys. Rev. B **95**, 075125 (2017).
- [9] T. C. Koethe, Z. Hu, M. W. Haverkort, C. Schüßler-Langeheine, F. Venturini, N. B. Brookes, O. Tjernberg, W. Reichelt, H. H. Hsieh, H.-J. Lin, C. T. Chen, and L. H. Tjeng, Phys. Rev. Lett. **97**, 116402 (2006).
- [10] H.-T. Kim, Y. W. Lee, B.-J. Kim, B.-G. Chae, S. J. Yun, K.-Y. Kang, K.-J. Han, K.-J. Yee, and Y.-S. Lim, Phys. Rev. Lett. **97**, 266401 (2006).
- [11] J. D. Budai, J. Hong, M. E. Manley, E. D. Specht, C. W. Li, J. Z. Tischler, D. L. Abernathy, A. H. Said, B. M. Leu, L. A. Boatner, R. J. McQueeney, and O. Delaire, Nature **515**, 535 (2014).
- [12] A. X. Gray, J. Jeong, N. P. Aetukuri, P. Granitzka, Z. Chen, R. Kukreja, D. Higley, T. Chase, A. H. Reid, H. Ohldag, M. A. Marcus, A. Scholl, A. T. Young, A. Doran, C. A. Jenkins, P. Shafer, E. Arenholz, M. G. Samant, S. S. P. Parkin, and H. A. Dürr, Phys. Rev. Lett. **116**, 116403 (2016).
- [13] J. H. Park, J. M. Coy, T. S. Kasirga, C. Huang, Z. Fei, S. Hunter, and D. H. Cobden, Nature **500**, 431 (2013).
- [14] N. B. Aetukuri, A. X. Gray, M. Drouard, M. Cossale, L. Gao, A. H. Reid, R. Kukreja, H. Ohldag, C. A. Jenkins, E. Arenholz, K. P. Roche, H. A. Dürr, M. G. Samant, and S. S. P. Parkin, Nat. Phys. **9**, 661 (2013).
- [15] M. Marezio, D. B. McWhan, J. P. Remeika, and P. D. Dernier, Phys. Rev. B **5**, 2541 (1972).
- [16] J. P. Pouget, H. Launois, T. M. Rice, P. Dernier, A. Gosard, G. Villeneuve, and P. Hagenmuller, Phys. Rev. B **10**, 1801 (1974).
- [17] E. Arcangeletti, L. Baldassarre, D. Di Castro, S. Lupi, L. Malavasi, C. Marini, A. Perucchi, and P. Postorino, Phys. Rev. Lett. **98**, 196406 (2007).
- [18] C. Marini, L. Baldassarre, M. Baldini, A. Perucchi, D. Di Castro, L. Malavasi, S. Lupi, and P. Postorino, High Press. Res. **30**, 55 (2010).
- [19] C. Marini, M. Bendele, B. Joseph, I. Kantor, M. Mitrano, O. Mathon, M. Baldini, L. Malavasi, S. Pascarelli, and P. Postorino, Europhys. Lett. **108**, 36003 (2014).
- [20] M. Baldini, P. Postorino, L. Malavasi, C. Marini, K. W. Chapman, and H.-k. Mao, Phys. Rev. B **93**, 245137 (2016).
- [21] L. Bai, Q. Li, S. A. Corr, Y. Meng, C. Park, S. V. Sologeikin, C. Ko, J. Wu, and G. Shen, Phys. Rev. B **91**, 104110 (2015).
- [22] Y. Chen, S. Zhang, F. Ke, C. Ko, S. Lee, K. Liu, B. Chen, J. W. Ager, R. Jeanloz, V. Eyert, and J. Wu, Nano Lett. **17**, 2512 (2017).
- [23] M. Mitrano, B. Maroni, C. Marini, M. Hanfland,

- B. Joseph, P. Postorino, and L. Malavasi, *Phys. Rev. B* **85**, 184108 (2012).
- [24] A. Cavalleri, C. Tóth, C. W. Siders, J. A. Squier, F. Ráksi, P. Forget, and J. C. Kieffer, *Phys. Rev. Lett.* **87**, 237401 (2001).
- [25] A. Cavalleri, T. Dekorsy, H. H. W. Chong, J. C. Kieffer, and R. W. Schoenlein, *Phys. Rev. B* **70**, 161102 (2004).
- [26] A. Cavalleri, M. Rini, H. H. W. Chong, S. Fourmaux, T. E. Glover, P. A. Heimann, J. C. Kieffer, and R. W. Schoenlein, *Phys. Rev. Lett.* **95**, 067405 (2005).
- [27] D. J. Hilton, R. P. Prasankumar, S. Fourmaux, A. Cavalleri, D. Brassard, M. A. El Khakani, J. C. Kieffer, A. J. Taylor, and R. D. Averitt, *Phys. Rev. Lett.* **99**, 226401 (2007).
- [28] C. Kübler, H. Ehrke, R. Huber, R. Lopez, A. Halabica, R. F. Haglund, and A. Leitenstorfer, *Phys. Rev. Lett.* **99**, 116401 (2007).
- [29] A. Pashkin, C. Kübler, H. Ehrke, R. Lopez, A. Halabica, R. F. Haglund, R. Huber, and A. Leitenstorfer, *Phys. Rev. B* **83**, 195120 (2011).
- [30] T. L. Cocker, L. V. Titova, S. Fourmaux, G. Holloway, H.-C. Bandulet, D. Brassard, J.-C. Kieffer, M. A. El Khakani, and F. A. Hegmann, *Phys. Rev. B* **85**, 155120 (2012).
- [31] S. Wall, D. Wegkamp, L. Foglia, K. Appavoo, J. Nag, R. Haglund, J. Stähler, and M. Wolf, *Nat. Commun.* **3**, 721 (2012).
- [32] D. Wegkamp, M. Herzog, L. Xian, M. Gatti, P. Cudazzo, C. L. McGahan, R. E. Marvel, R. F. Haglund, A. Rubio, M. Wolf, and J. Stähler, *Phys. Rev. Lett.* **113**, 216401 (2014).
- [33] V. R. Morrison, R. P. Chatelain, K. L. Tiwari, A. Hendaoui, A. Bruhacs, M. Chaker, and B. J. Siwick, *Science* **346**, 445 (2014).
- [34] B. T. O’Callahan, A. C. Jones, J. Hyung Park, D. H. Cobden, J. M. Atkin, and M. B. Raschke, *Nat. Commun.* **6**, 6849 (2015).
- [35] M. A. Huber, M. Plankl, M. Eisele, R. E. Marvel, F. Sandner, T. Korn, C. Schüller, R. F. Haglund, R. Huber, and T. L. Cocker, *Nano Lett.* **16**, 1421 (2016).
- [36] W.-P. Hsieh, M. Trigo, D. A. Reis, G. A. Artioli, L. Malavasi, and W. L. Mao, *Appl. Phys. Lett.* **104**, 021917 (2014).
- [37] See Supplemental Material below for detailed information about the growth of the VO₂ single crystals, the bi-asymptotic fit describing the pump–probe amplitude as function of pump fluence [see Fig. 1(c) and (d)], our Raman measurements on a pressurized VO₂ crystal and discussion of special features observed in the measurement data.
- [38] H. K. Mao, J. Xu, and P. M. Bell, *J. Geophys. Res.* **91**, 4673 (1986).
- [39] M. F. Becker, A. B. Buckman, R. M. Walser, T. Lépine, P. Georges, and A. Brun, *Appl. Phys. Lett.* **65**, 1507 (1994).
- [40] N. F. Brady, K. Appavoo, M. Seo, J. Nag, R. P. Prasankumar, R. F. Haglund, and D. J. Hilton, *J. Phys. Condens. Matter* **28**, 125603 (2016).
- [41] X. Y. Zhang, M. J. Rozenberg, and G. Kotliar, *Phys. Rev. Lett.* **70**, 1666 (1993).
- [42] D. I. Khomskii, *Transition Metal Compounds* (Cambridge University Press, Cambridge, 2014).
- [43] Z. He and A. J. Millis, *Phys. Rev. B* **93**, 115126 (2016).
- [44] W. H. Brito, M. C. O. Aguiar, K. Haule, and G. Kotliar, *Phys. Rev. Lett.* **117**, 056402 (2016).

Supplemental material for "Ultrafast Carrier Dynamics in VO₂ across the Pressure-Induced Insulator-to-Metal Transition"

Johannes M. Braun,^{1,2,*} Harald Schneider,¹ Manfred Helm,^{1,2} Rafał Mirek,³
Lynn A. Boatner,⁴ Robert E. Marvel,⁵ Richard F. Haglund,⁵ and Alexej Pashkin^{1,†}

¹Helmholtz-Zentrum Dresden-Rossendorf, P.O. Box 510119, 01314 Dresden, Germany

²Technische Universität Dresden, 01062 Dresden, Germany

³Faculty of Physics, University of Warsaw, Pasteura 5, PL-02-093 Warsaw, Poland

⁴Oak Ridge National Laboratory, P.O. Box 2008, Oak Ridge, TN 37831, USA

⁵Vanderbilt University, Department of Physics and Astronomy, Nashville, TN 37235-1807, USA

(Dated: March 13, 2022)

DETERMINATION OF THE THRESHOLD PARAMETERS

In order to determine the threshold fluence we fit the fluence dependence of the pump-probe signal at the delay time of 1 ps. For this purpose we use a phenomenological fit function with bi-asymptotic behavior:

$$\frac{\Delta R}{R}(\Phi) = c \ln [a e^{s_1 \Phi} + (1-a) e^{s_2 \Phi}], \quad (1)$$

with four independent positive fit parameters c , a , s_1 and s_2 . In the limit of very large or very small fluences one of the exponential terms dominates, and the fit function demonstrates a nearly linear dependence on Φ .

The threshold fluence Φ_{th} is defined as a fluence at which the second derivative $\partial^2 \frac{\Delta R}{R} / \partial^2 \Phi$ is maximal, i.e., the fit curve has the highest curvature. It can be shown that this condition implies the equality of both exponential terms in Eq. (1) and, thus

$$\Phi_{\text{th}} = \frac{1}{s_2 - s_1} \ln \left(\frac{a}{1-a} \right). \quad (2)$$

In order to achieve a stable operation of the numerical fitting procedure an equivalent version of Eq. (1) was used:

$$\frac{\Delta R}{R}(\Phi, \Delta t = 1 \text{ ps}) = c \ln \left[\frac{e^{s_3 \Phi_{\text{th}}}}{1 + e^{s_3 \Phi_{\text{th}}}} e^{s_1 \Phi} + \left(1 - \frac{e^{s_3 \Phi_{\text{th}}}}{1 + e^{s_3 \Phi_{\text{th}}}} \right) e^{(s_1 + s_3) \Phi} \right], \quad (3)$$

where the parameter a that exponentially approaches 1 is replaced by the well-defined threshold fluence Φ_{th} . Also a new parameter $s_3 = s_2 - s_1$ is introduced for simplicity.

With the fit parameters Φ_{th} , c , s_1 , s_3 , the slope of the low-fluence asymptote m_1 can be derived by neglecting the second exponential term in Eq. (3):

$$m_1 = c s_1 \quad (4)$$

The width of the transition between the low- and the high-fluence asymptotes can be estimated as the full

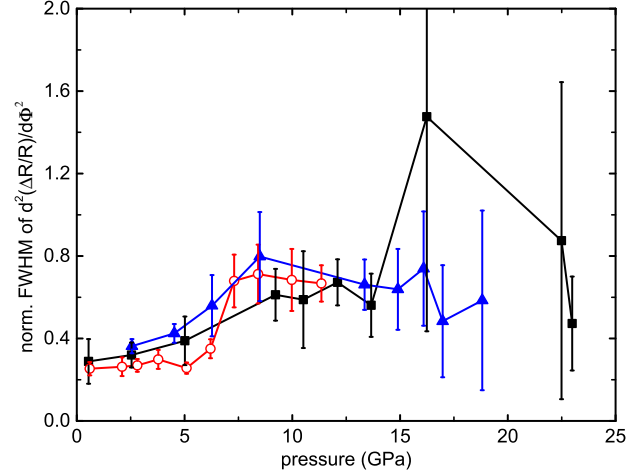


FIG. S1. Pressure dependence of the FWHM parameter from Eq. (5) normalized to the threshold fluence $\Phi_{\text{th}}(p)$.

width at half maximum (FWHM) of the second derivative of $\Delta R/R(\Phi)$ with respect to the fluence Φ . One can show that

$$\text{FWHM} = \frac{2}{s_3} \ln \left(\frac{\sqrt{2} + 1}{\sqrt{2} - 1} \right) \quad (5)$$

Thus, the FWHM is determined just by the fit parameter s_3 . Figure S1 shows how the unsharpness of the threshold behavior (ratio of the FWHM to the threshold fluence) changes with pressure. The pressure-induced metallization leads to a less sharp threshold behavior due to the onset of a finite slope m_1 and the drop in the threshold fluence. Nevertheless, the threshold behavior remains sufficiently sharp in the whole studied pressure range. The larger error bars at the high pressures are a consequence of weak pump-probe signals and low threshold values.

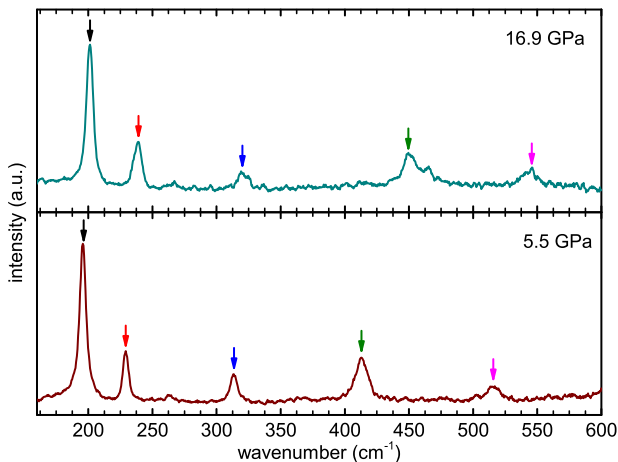


FIG. S2. Raman spectra of VO₂ at 5.5 GPa (brown) and 16.9 GPa (cyan). Arrows mark the positions of the phonon modes plotted in Fig. S3.

RAMAN MEASUREMENTS ON PRESSURIZED VO₂

Pressure-dependent Raman measurements were performed on a tiny, 10 μm thick single VO₂ crystal with 4:1 methanol-ethanol mixture as a pressure transmitting medium. Figure S2 shows Raman spectra at selected pressures below and above the IMT. The same set of phonon peaks can be observed up to the highest pressure indicating that the monoclinic structure is preserved. In contrast to the temperature-driven IMT, we do not observe a signature of the rutile metallic phase, where the sharp Raman peaks just disappear [1].

Figure S3 shows the frequencies of Raman modes as function of pressure. The kinks around 12 GPa indicating an isostructural phase transition are in agreement with literature [2–5].

VO₂ SINGLE CRYSTALS

The single crystals of VO₂ [see Fig. S4] were grown at the Oak Ridge National Laboratory using the methods described in Ref. [6] and used in both Raman and pump-probe measurements.

NEGATIVE PUMP-PROBE SIGNAL AT SMALL NEGATIVE DELAY TIME

Below the critical pressure p_c a small negative pump-probe signal is observed for negative delay times around 0.5 ps getting more prominent for higher pump fluences [see Fig. 1(a)]. The origin of this feature is related to a pump-induced suppression of a portion of the probe pulse that is reflected from the backside of the sample.

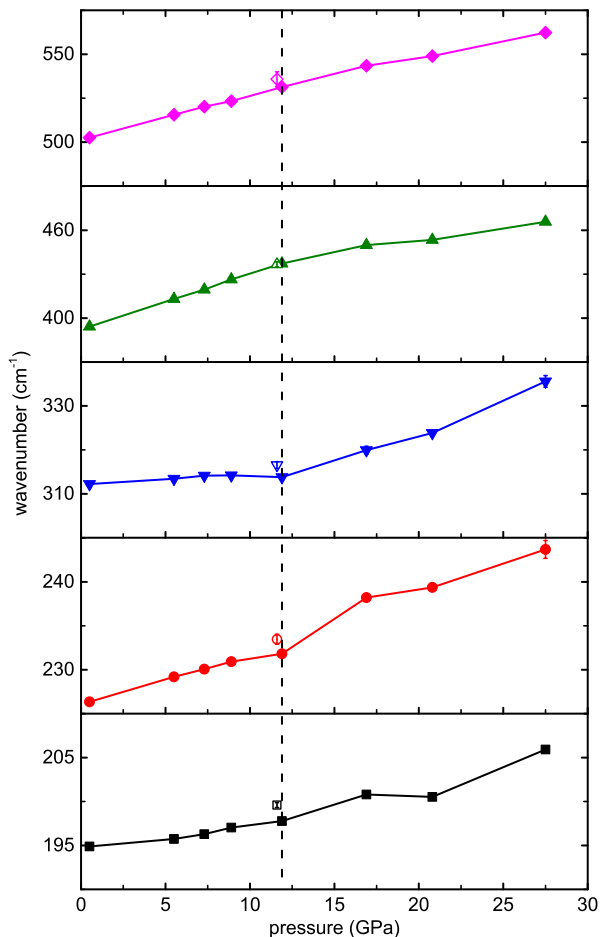


FIG. S3. Pressure dependence of selected Raman modes in VO₂. The open symbol corresponds to a Raman spectrum that was captured after the release of pressure. Color coding corresponds to the arrow markers in Fig. S2.



FIG. S4. Single crystals of VO₂

Initially the sample is transparent for the probe light, but when the portion reflected from the backside of the sample arrives the front surface excited by the pump pulse, its transmission is decreased by the layer of photo-excited free charge carriers. For fluences above the threshold the surface layer is metallic, and the suppression is very efficient. A rough estimation with a sample thickness of 20-30 μm and refractive index of VO_2 around 3.2 [7] results in the observed delay time of -0.5 ps, which corresponds to temporal overlap of the probe pulse after the round trip through the sample with the incident pump pulse.

In the pressure-induced metallic phase the transmissivity of the sample vanishes and no light reflected from the backside of the sample can be detected. Therefore, the artifact at the negative delay time cannot be observed anymore for any pump fluence. Thus, the missing negative pump-probe signal beyond 6-8 GPa is another evidence for a pressure-induced metallic phase [see Fig. 3(d)].

RELAXATION TIMESCALES IN PHOTO-EXCITED VO_2

The relaxation time constants of photo-excited charge carriers in pressurized VO_2 can be determined by mono-exponential fitting of the pump-probe traces at delay times between 0.05 and 1.0 ps. In Fig. S5 the time constants obtained from pump-probe traces corresponding to pump fluences within an interval of 5 mJ/cm^2 below the threshold Φ_{th} are shown. The pump-probe traces measured at these fluences provide the most reliable estimation of the relaxation time: At lower fluences the signal-to-noise ratio is worse and at pump fluences beyond the threshold the long-lived signal affects the fitting. In general, we observe that the relaxation time is weakly dependent on the pump fluence.

The relaxation time constants for all three studied samples have pressure-independent values scattered in the range of 0.15 to 0.20 ps. Previous study demonstrated similar values of the decay time [8]. There might be a weak pressure dependence with slightly shorter relaxation time constants at pressures beyond 16 GPa. However, this could be an artifact caused by a decreased signal-to-noise ratio for the data taken at highest pressures where the signal amplitude becomes very low.

ENHANCED PHOTOSUSCEPTIBILITY IN THE PRESSURE-INDUCED METALLIC PHASE

The amplitude of the pump-probe signal clearly increases at the critical pressure. This effect of enhanced photosusceptibility is illustrated in Fig. S6, where the pump-probe amplitude for constant pump fluence

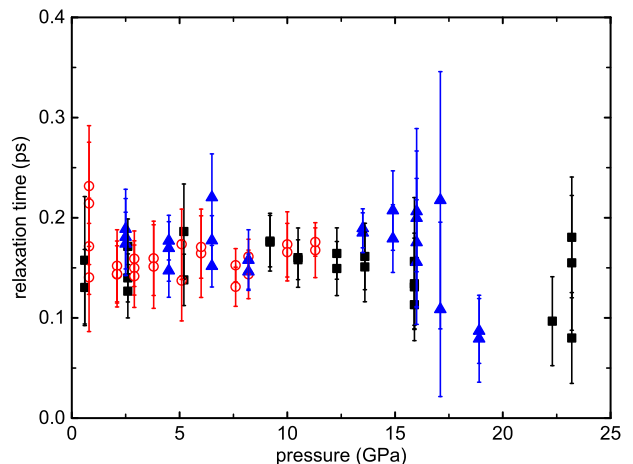


FIG. S5. Fitted relaxation time constants for pump-probe traces corresponding to pump fluences within an interval of 5 mJ/cm^2 below the threshold Φ_{th} as function of pressure.

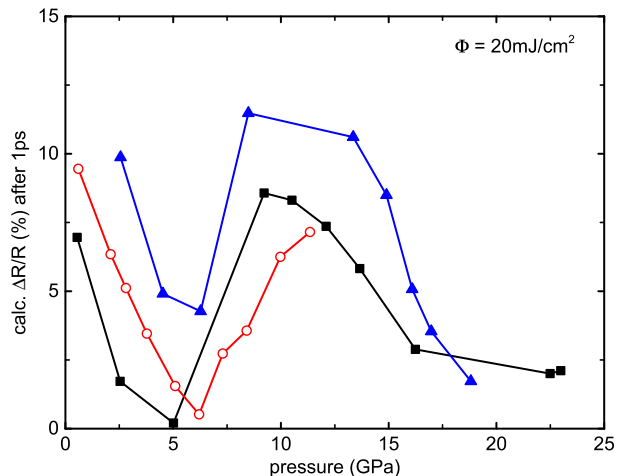


FIG. S6. Pressure-dependence of the pump-probe amplitude for a constant pump-fluence $\Phi = 20 \text{ mJ/cm}^2$. The traces are calculated with the parameters obtained from the threshold fitting and correspond to the three samples analyzed in Fig. 2.

$\Phi = 20 \text{ mJ/cm}^2$ is plotted as a function of pressure. Here we utilized the pressure-dependent parameters obtained from the threshold fitting to calculate the pump-probe signal at a delay time of 1 ps for particular pressures.

Starting from ambient conditions, for all three samples the pump-probe signal decreases until the critical pressure is reached. This behavior as well as the sudden increase of the pump-probe amplitude beyond the critical pressure is a direct consequence of the first increasing and then dropping threshold fluence. The decrease of the pump-probe signal $\Delta R/R$ at even higher pressures can be explained by the rising number of pressure-induced free charge carriers, as then the photo-induced relative

change in the density of free charge carriers lowers.

Enhanced photosusceptibility also was found for the temperature-driven IMT [9], but on the other side of the phase transition. While we observed this enhancement in the metallic phase, for the temperature-driven IMT it appears in the insulating phase. There the enhancement is due to the lowered thermodynamic barrier between the monoclinic and rutile phase when the monoclinic phase is heated [9, 10].

* j.braun@hzdr.de

† a.pashkin@hzdr.de

- [1] P. Schilbe, *Phys. B* **316-317**, 600 (2002).
- [2] E. Arcangeletti, L. Baldassarre, D. Di Castro, S. Lupi, L. Malavasi, C. Marini, A. Perucchi, and P. Postorino, *Phys. Rev. Lett.* **98**, 196406 (2007).
- [3] C. Marini, L. Baldassarre, M. Baldini, A. Perucchi, D. Di Castro, L. Malavasi, S. Lupi, and P. Postorino, *High Press. Res.* **30**, 55 (2010).
- [4] M. Mitrano, B. Maroni, C. Marini, M. Hanfland, B. Joseph, P. Postorino, and L. Malavasi, *Phys. Rev. B* **85**, 184108 (2012).
- [5] L. Bai, Q. Li, S. A. Corr, Y. Meng, C. Park, S. V. Sino-geikin, C. Ko, J. Wu, and G. Shen, *Phys. Rev. B* **91**, 104110 (2015).
- [6] J. D. Budai, J. Hong, M. E. Manley, E. D. Specht, C. W. Li, J. Z. Tischler, D. L. Abernathy, A. H. Said, B. M. Leu, L. A. Boatner, R. J. McQueeney, and O. Delaire, *Nature* **515**, 535 (2014).
- [7] A. S. Barker, H. W. Verleur, and H. J. Guggenheim, *Phys. Rev. Lett.* **17**, 1286 (1966).
- [8] C. Kübler, H. Ehrke, R. Huber, R. Lopez, A. Halabica, R. F. Haglund, and A. Leitenstorfer, *Phys. Rev. Lett.* **99**, 116401 (2007).
- [9] D. J. Hilton, R. P. Prasankumar, S. Fourmaux, A. Cavalleri, D. Brassard, M. A. El Khakani, J. C. Kieffer, A. J. Taylor, and R. D. Averitt, *Phys. Rev. Lett.* **99**, 226401 (2007).
- [10] A. Pashkin, C. Kübler, H. Ehrke, R. Lopez, A. Halabica, R. F. Haglund, R. Huber, and A. Leitenstorfer, *Phys. Rev. B* **83**, 195120 (2011).